MAY 2014 VOL 10 NO 5
www.nature.com/naturephysics

nature physics

Graphene as supporting act

BEYOND GRAPHENE
Valley physics in dichalcogenides

HOLOGRAPHIC DUALITY
Quantum criticality in real time

SYNCHROTRON RADIATION
Fast cooling for prompt γ-ray-burst emission

ARTICLES
PUBLISHED ONLINE: 30 MARCH 2014 | DOI: 10.1038/NPHYS2929
nature physics

Collapse of superconductivity in a hybrid tin–graphene Josephson junction array

Zheng Han[1,2], Adrien Allain[1,2], Hadi Arjmandi-Tash[1,2], Konstantin Tikhonov[3,4], Mikhail Feigel'man[3,5], Benjamin Sacépé[1,2] and Vincent Bouchiat[1,2]*

For a Josephson junction array with hybrid superconductor/metal/superconductor junctions, a quantum phase transition from a superconducting to a two-dimensional (2D) metallic ground state is predicted to occur on increasing the junction normal state resistance. Owing to its surface-exposed 2D electron gas and its gate-tunable charge carrier density, graphene coupled to superconductors is the ideal platform to study such phase transitions between ground states. Here, we show that decorating graphene with a sparse and regular array of superconducting discs enables the continuous gate-tuning of the quantum superconductor-to-metal transition of the Josephson junction array into a zero-temperature metallic state. The suppression of proximity-induced superconductivity is a direct consequence of the emergence of quantum fluctuations of the superconducting phase of the discs. Under perpendicular magnetic fields, the competition between quantum fluctuations and disorder is responsible for the resilience of superconductivity at the lowest temperatures, supporting a glassy state that persists above the upper critical field. We provide the entire phase diagram of the disorder and magnetic-field-tuned transition to reveal the role of quantum phase fluctuations in 2D superconducting systems.

The nature of the ground state terminating 2D superconductivity in the superconductor–(metal)–insulator quantum phase transition has been a central issue in condensed matter physics[1], which still remains unresolved today[2]. In granular[3,4] and in some amorphous superconducting thin films[5–10], oxide interfaces[11,12] and Josephson junction arrays[13,14], an intervening metallic state is often observed experimentally at the disorder-tuned or magnetic field-tuned quantum critical point separating the superconducting from the (weak) insulating state. In contrast to usual non-interacting 2D electronic systems, in which electron localization yields an insulating ground state[15], this metallic state is characterized by the presence of electron-pairing fluctuations that are indicated in experiments by a partial drop of resistance—reminiscent of the nearby superconducting phase—preceding the nearly T-independent resistive state.

The possibility that a 2D system can undergo a zero-temperature superconducting to metal transition is indeed rather intriguing[16–22]. The physics of this metallic state, sometimes termed as a Bose metal[18,21], in which charge carriers are supposedly condensed in Cooper pairs, is not clear. Considerable theoretical efforts have been focused on the role of quantum phase-fluctuations of the superconducting order parameter in the regime where the superconducting phase stiffness breaks down. In particular, models involving specific types of Josephson junction arrays in which superconducting discs are coupled together via a 2D disordered metal through the proximity effect have been considered[16,17,20,22]. Such proximity-coupled arrays encompass all the physical ingredients: conventional superconducting electron pairing, embedded dissipation channels in the normal disordered metal, and quantum fluctuations of superconducting phases due to a weak Coulomb blockade on superconducting discs[23].

The theoretical analysis of these models shows that a quantum phase transition from a superconducting state to a non-superconducting state can be tuned by two different means: either geometrically by increasing the distance between discs, or by increasing the metal resistance. Both parameters directly affect the superconducting proximity effect and result in a marked enhancement of quantum phase fluctuations. Although the proximity effect is expected to extend over infinite distance at zero temperature, leading systematically to a superconducting ground state, the main conclusion of recent theories[16,17,20,22] is that quantum phase fluctuations lead to a collapse of superconductivity, that is, of the array phase stiffness. This should arise at a given critical value of the tuning parameter, leading to a zero-temperature 2D metallic state.

On the experimental side, it is hardly conceivable to access this quantum breakdown of superconductivity by tuning continuously the resistance of a metallic thin film that carries the superconducting proximity effect. Varying the inter-disc distance on a large set of samples has thus remained the only reliable approach with thin films. A recent study of proximity arrays consisting of gold thin-films covered with an array of niobium nano-discs[24] has demonstrated that the critical temperature of such proximity-coupled arrays decreases on increasing the inter-disc distance and extrapolates to zero for a finite inter-disc distance, suggesting a quantum phase transition to a non-superconducting, metallic ground state.

In this work, we take a different route to tune the quantum phase transition in a controllable fashion. We use graphene[25], a purely 2D crystal of carbon atoms, to serve as the diffusive metal, which we decorate with a triangular array of tin discs (a type-I superconductor). The gate-tunable sheet resistance of graphene, which can approach the quantum of resistance (h/e^2), enables us to continuously vary the strength of disorder, which affects the inter-disc proximity effect, and therefore tune the transition from the superconducting to the metallic state. Furthermore, the charge-carrier density of graphene is always several orders of magnitude below those of classical metals, preventing the weakening of the

[1]Univ. Grenoble Alpes, Institut Néel, F-38042 Grenoble, France, [2]CNRS, Institut Néel, F-38042 Grenoble, France, [3]L. D. Landau Institute for Theoretical Physics, Kosygin street 2, Moscow 119334, Russia, [4]Department of Condensed Matter Physics, The Weizmann Institute of Science, 76100 Rehovot, Israel, [5]Moscow Institute of Physics and Technology, Moscow 141700, Russia. *e-mail: vincent.bouchiat@grenoble.cnrs.fr

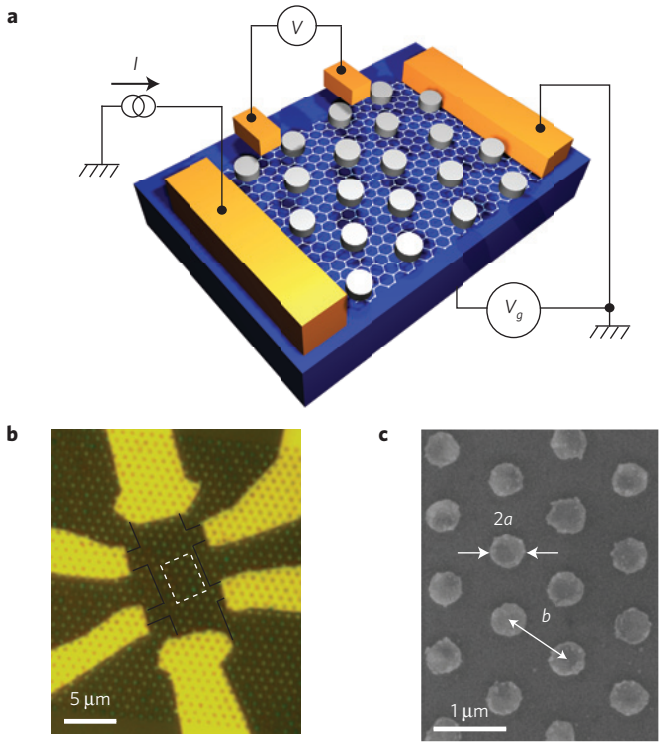

Figure 1 | Proximity-coupled array of superconducting discs on graphene. **a**, Schematics of the device, involving a triangular array of superconducting tin discs decorating the bare graphene surface. The device is connected to a current source and measured using a four-probe measurement set-up. **b**, Optical micrograph of the sample. The black lines indicate the graphene sample plasma-etched Hall bar, which is connected to the gold electrodes seen on the edge of the image. The graphene surface is decorated with a regular array of tin discs of diameter 400 nm, separated by 1 μm between centres. **c**, Scanning electron micrograph of the dashed rectangular region in **b** showing the triangular lattice of tin discs with diameter $2a$ and separated by a distance b.

superconductivity on the discs by the inverse proximity effect[26]. As we describe below, these capabilities, along with quantitative comparisons with theory, allow us to reveal both the collapse of superconductivity by quantum phase fluctuations, and the ensuing 2D metallic state. In addition, under perpendicular magnetic field a re-entrant superconducting state is observed at our lowest temperatures, as expected from theory[27–29].

Berezinskii–Kosterlitz–Thouless transition

Our proximity-induced array consists of a triangular lattice of disc-shaped superconducting islands, which are deposited onto a graphene Hall bar equipped with a backgate electrode (Fig. 1). The superconducting discs are in the form of 50 nm thick tin films, with diameter $2a = 400$ nm. Discs are separated by a distance $b = 1$ μm between their centres (Fig. 1). The electron mobility of the graphene extracted from a fit of the field effect and from Hall measurements is 680 cm^2 V^{-1} s^{-1} at high gate voltages (Supplementary Fig. 1), while the mean free path l can be varied with the backgate in the range 10–30 nm (Supplementary Fig. 2), corresponding to a diffusion coefficient $D = 50$–140 cm^2 s^{-1} (Supplementary Fig. 2). Our system differs considerably from previous experiments performed on tin–graphene hybrids[4,30], for which tin clusters of random shapes densely self-assembled on the graphene surface by dewetting. Those experiments were performed in the opposite regime of short junctions (coherence length $\gg b$) and in one case[4] in the limit of strongly disordered graphene (mean free path $\ll b$), for which a superconductor-to-insulator quantum phase transition has been observed on decreasing the graphene charge carrier density.

We begin the presentation of the data by describing the two-step transition[31,32] that the sample undergoes towards the superconducting state. On cooling from the normal state, a gate-independent resistance drop occurs at a temperature of ~3.6 K (Fig. 2a, red and blue curves, also Supplementary Fig. 3), which is consistent with a previous observation of the superconducting transition temperature of tin nanoparticles[30]. We attribute this first drop to the superconducting transition of the discs, which locally shunt the graphene area underneath. The relative resistance drop $\Delta R/R_N$ at this transition amounts to 20% on the electron side and 10% on the hole side, in good agreement with a model including a carrier dependent tin/graphene interface transparency (Supplementary Information). Such an electron/hole asymmetry is related to the pinning of the charge density of graphene below the metal[33], which in the case of tin[30] leads to a p/n junction on the hole side and a transparent p/p junction on the electron side. In the rest of the paper, we will focus rather on the electronic properties of the system on the electron side, for which the relative drop of resistance $\Delta R/R_N$ exceeds the filling factor of the tin deposition (Supplementary Fig. 3), indicating that the tin/graphene interface conductance greatly exceeds the quantum of conductance.

Further cooling enhances the proximity effect via the graphene, which eventually leads to the percolation of superconductivity and the establishment of a 2D superconducting state (Supplementary Fig. 3a,b). As shown in Fig. 2a, at gate voltages between 0 and 30 V, the resistance decreases when the temperature is lowered from 3 K to 0.06 K. An opposite trend is seen for gate voltages close to the charge neutrality point (namely, from −30 V to 0 V).

Below 1 K and for gate voltages above −3 V, the proximity-coupled array develops full superconductivity, with a zero resistance state and a gate-dependent critical temperature. The transition is captured by a Berezinskii–Kosterlitz–Thouless (BKT) mechanism[34,35], which describes the 2D superconducting transition as a proliferation and unbinding, at T_c^{BKT}, of vortex–antivortex pairs, that is, thermal phase fluctuations of the superconducting order parameter. A colour-scaled map showing the device resistance versus gate voltage and temperature is shown in Fig. 2b. The experimentally measured superconducting temperature T_c is indicated by the white contour. The higher positive gate voltage leads to higher T_c, whereas T_c vanishes in the region around the charge neutrality point, between −30 V and −3 V.

For Josephson junction arrays, the value of T_c^{BKT} is directly proportional to the Josephson energy $E_J(b,T)$ of a single junction formed between two superconducting discs. For a triangular lattice, the relation reads[29]:

$$T_c^{BKT} \simeq 1.47\, E_J(b, T_c^{BKT}) \qquad (1)$$

where $E_J(b,T)$ depends on the metal conductance g, the inter-disc distance b and the diffusion coefficient D (Methods). Using experimentally extracted values of D and of the graphene resistance measured at 4 K for all back-gate values, we calculated T_c^{BKT} by solving (1) self-consistently with respect to T for the entire back-gate range (Methods). In Fig. 2b, the resulting T_c^{BKT} is shown by the dashed line. For high gate voltages (that is, $V_g > 10$ V) this theoretical value of T_c^{BKT} is in excellent agreement with the experimental critical temperature T_c without any fitting parameter, supporting the theoretical model[29].

The critical supercurrent at $T = 0$ provides another computable physical quantity in such arrays. As shown in Fig. 3a, the plot of the differential resistance dV/dI versus bias current and V_g allows us to obtain the full V_g dependence on I_c at $T = 0.06$ K. In the zero-temperature limit, the critical current of an array of discs can be inferred from the Josephson coupling energy of neighbouring

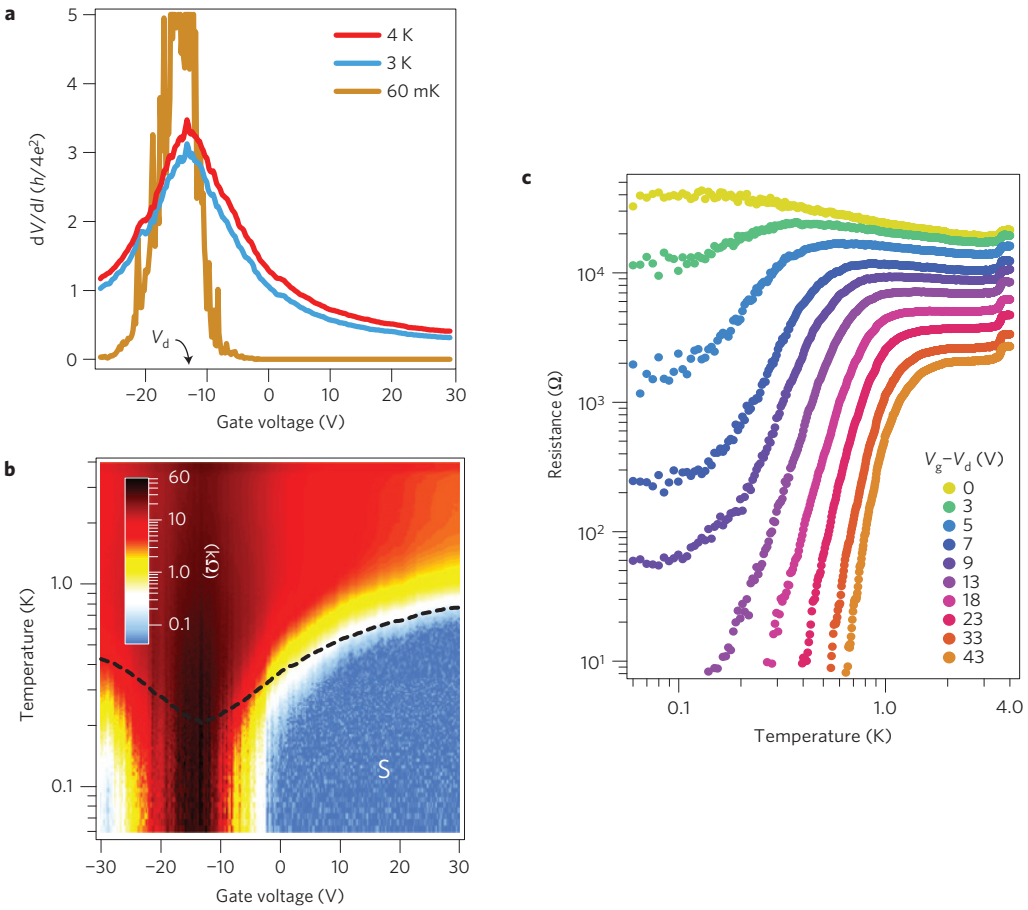

Figure 2 | Collapse of superconductivity in the proximity-coupled array. a, Gate voltage dependence of the four-probe resistance for three different temperatures. The curve at $T = 4$ K gives the gate dependence of the device resistance above the superconducting transition of the tin discs. At $T = 3$ K, the resistance drops throughout the full gate range owing to the superconducting transition of the tin discs. At the base temperature of 0.06 K, the array undergoes a transition from the superconducting to the resistive state for $-29\,\text{V} < V_g < -3\,\text{V}$ and the resistance exhibits a sharp peak at the charge neutrality point, indicated by V_d, the so-called Dirac voltage. **b**, Colour-scaled map of resistance versus temperature and gate voltage (V_g). The superconducting phase (S) on the electron-doped side is shown as the blue area and the superconducting critical temperature T_c bordering the resistive state is indicated by the white contour. The dashed line is calculated from equation (1) without a fitting parameter. The experimental T_c deviates around $V_g = 5$ V towards a sharp breakdown of the superconducting state at $V_g = -3$ V. **c**, Line cuts from **b** of the temperature dependence of the array resistance. Whereas the resistance drops into a fully superconducting state for $V_g - V_d > 10$ V, a levelling-off to a gate-dependent finite value is observed for $0 < V_g - V_d < 10$ V.

discs[29], which is given by:

$$E_J(b, T=0) = \frac{\pi^3}{4}\frac{g\hbar D}{b^2 \ln^2(b/a)} = \frac{\hbar}{2e} I_1 \qquad (2)$$

where $g = \hbar/(e^2 R_\square)$ is the dimensionless conductance of graphene in the normal state, with $R_\square$ the sheet resistance, and I_1 is the maximum supercurrent between two neighbouring discs. The total critical current I_c can be estimated by summing the local critical current I_1 of each of the disc neighbours (Fig. 1b) of the array, which contribute as parallel channels, and by neglecting the small contribution to I_c from non-nearest pairs of discs, leading to: $I_c \approx 6I_1$. According to the above relations, at $T \ll T_c$, the product of $I_c R_N$ (R_N being the graphene sheet resistance in the normal state) should depend only on diffusion coefficient D for a given geometry. This can be directly tested, as the use of graphene as a 2D disordered metal enables one to gate-tune the diffusion coefficient while keeping all geometrical aspects of the array constant. By extracting the experimental critical current I_c from Fig. 3a, and measuring R_N at 4 K (Fig. 2a), we plot the quantity $eI_cR_N/\hbar D$ as a function of the gate voltage in Fig. 3b. One can see that above a given doping level this quantity reaches a constant level of $3.6\times10^9\,\text{cm}^{-2}$. Such a value matches the quantity $3\pi^3/b^2\ln^2(b/a)$ (dashed line in Fig. 3b), which depends only on the geometry of the array. Therefore, at high gate voltages, this experiment follows the theoretical predictions for such proximity-coupled arrays of discs sparsely decorating graphene[29].

Quantum breakdown of superconductivity

The central result of this work is the anomalous reduction of the sample's critical temperature T_c with respect to the calculated T_{BKT} on increasing graphene resistance, leading to a sudden collapse of superconductivity when approaching the charge neutrality point of the graphene layer (dark red region of Fig. 2b). The V_g-dependence of T_c shown in Fig. 2b first deviates from T_c^{BKT} towards lower temperatures for $V_g < 10$ V, and then abruptly drops to zero at around -3 V. The suppression of superconductivity is also apparent in the V_g-dependence of the critical supercurrent I_c at 0.06 K. As can be seen in Fig. 3, the zero-resistance state (blue region, marked as 'S' in Fig. 3a) disappears when $V_g = -3$ V, in a similar fashion as for T_c. We attribute these significant deviations, culminating in the collapse of superconductivity, to the failure of the BKT model[29], which takes into account only thermal phase fluctuations.

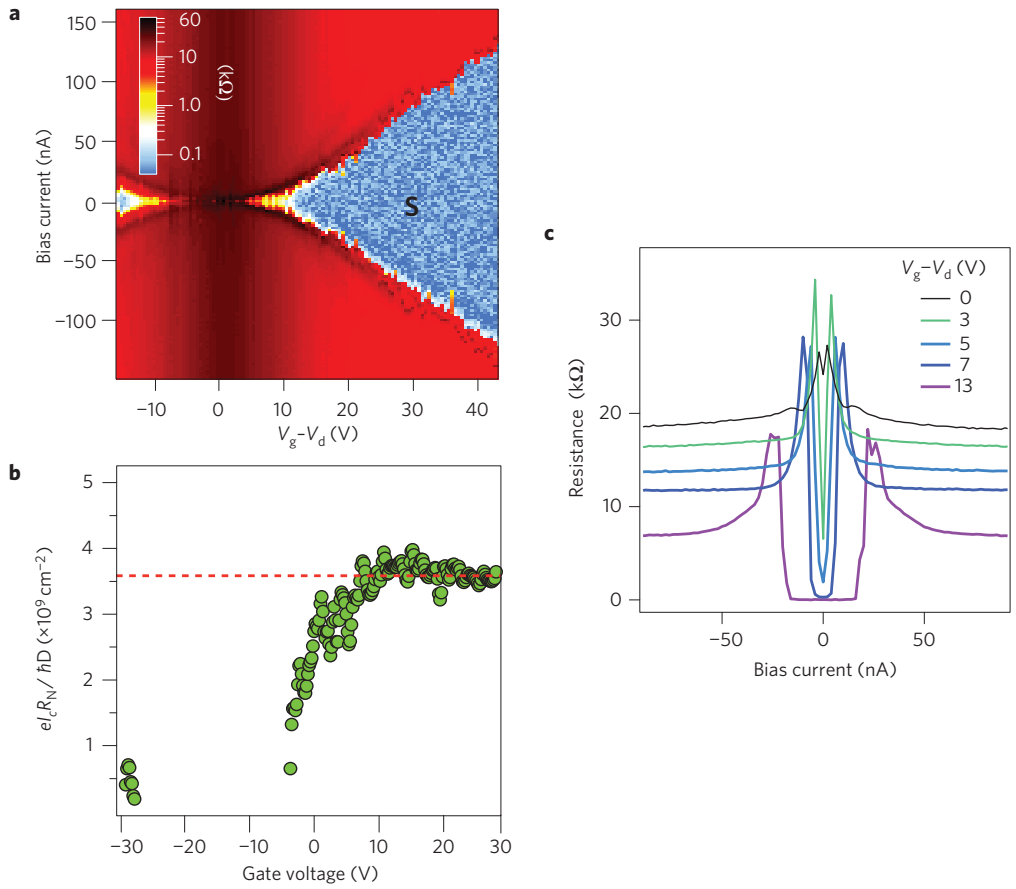

Figure 3 | Critical current in the proximity-coupled array at 0.06 K. a, Colour-scaled map of the differential resistance dV/dI measured at 0.06 K versus the gate voltage (with respect to the Dirac voltage) and bias current. The border between the zero-resistance state (blue area) and the resistive state (red area) indicates the critical current I_c. **b**, The quantity $el_cR_N/\hbar D$ calculated from the data of (**a**) and from Supplementary Fig. 2, plotted as a function of the gate voltage. The red dotted line corresponds to the theoretical value calculated using equation (2) **c**, Line cuts of **a**: current-biased differential resistance measured at 0.06 K for a set of gate voltages ranging from −13 V to 0 V.

Therefore our results are a direct consequence of the breakdown of the superconducting phase stiffness due to the emergence of quantum phase fluctuations[16,17,29].

The quantum origin of phase fluctuations in such proximity-coupled arrays stems from the particle number–phase uncertainty relation, which states that when the number of particles in an isolated superconducting disc is fixed, the phase of the superconducting order parameter will undergo strong non-thermal fluctuations. In tunnelling Josephson junction arrays, such quantum phase fluctuations are expected to occur when the disc charging energy overcomes the Josephson coupling energy[13], a situation that leads to charge quantization and the Coulomb blockade of the tunnelling into the discs.

Proximity-coupled arrays behave differently because their superconducting discs are coupled well to a metal layer without a tunnel barrier. When the normal-state resistance of the array approaches a few kΩ, which is achievable with graphene, the Andreev conductance—that is, the conductance for electron pairs—can be such that a weak charge quantization[23] of charge $2e$ prohibits the charge transfer into the discs. As the transfer of quasiparticles is also hindered at $T \ll T_c$ by the superconducting gap, the total charge of the discs tends to become fixed and thus promotes quantum fluctuations of the phase of the superconducting order parameter, as considered in refs 16,17, where this effect was analysed taking into account dissipation in normal regions between superconducting discs. Note that dissipation was identified as a critical parameter in the analysis of the superconducting to metal transition in MoGe thin films[6]. As a result, theory predicts that the presence of quantum phase fluctuations leads to an effective decoupling of superconducting phases between discs, and eventually to the collapse of the array phase stiffness for a given critical resistance of the 2D metal[16,17]. In our system, the wide range of tunability of graphene sheet resistance is the key ingredient allowing access to this regime of weak charge quantization and the ensuing superconducting-metal transition.

We next investigate the nature of the state terminating superconductivity near the charge neutrality point (that is, for $V_g - V_d < 10$ V). We systematically measured the temperature dependence of the resistance (R–T curves). In the non-superconducting regime (Fig. 2c), they exhibit a resistance drop below 0.5 K reminiscent of the superconducting transition observed for higher gate voltages, which indicates that superconducting fluctuations have developed in the graphene. However, instead of falling into a zero-resistance superconducting state, the R–T curves level off at finite, gate-dependent values that reach up to 28 kΩ at the charge neutrality point. Importantly, we can exclude the possibility of electron heating as the origin of this metallic tail at low temperature because, under a magnetic field of 30 mT, the levelling-off disappears (Supplementary Fig. 4).

To obtain further insights into this critical regime in Fig. 3c we show a set of curves for the differential resistance versus bias current extracted from the data of Fig. 3a for a few values of V_g. In the superconducting state, zero resistance is observed up to the critical current, as discussed before. However, for $V_g < -3$ V, where

the R–T curves saturate at finite values on cooling, the differential resistance around zero current bias transform into a zero-bias dips that persist even close to the charge neutrality point at the Dirac voltage $V_d = -13$ V. These dips give a clear indication that superconducting fluctuations exist for all gate voltages. Therefore, we are led to conclude that the ground state of our array, which exhibits finite resistance at the zero-temperature limit, is related to superconductivity. Moreover, the fact that the R–T curves conspicuously extrapolate to a constant resistance at zero temperature suggests that a 2D quantum metallic state is approached. We believe that the nature of this collapse of superconductivity and the resulting quantum metallic state arise from the enhancement of quantum phase fluctuations on increasing graphene resistance, eventually leading to the effective decoupling of the discs' superconducting phases. For critical temperatures below the typical Thouless energy of a single junction, $E_{Th} = \hbar D/b^2$, the impact of quantum fluctuations on T_c is expected[17] to be pronounced, with an exponential suppression in the form $T_c \sim E_{Th} \exp(-c/(g-g_c))$, where g_c is the critical conductance of graphene and c is a constant, which qualitatively explains the observed collapse of superconductivity.

Furthermore, the variation with gate voltage of the finite resistance saturating at the zero-temperature limit in the metallic state ($V_g < -3$ V) may be partially attributed to superconducting fluctuations of Aslamazov–Larkin[36] and Maki–Thompson[37,38] types, which would include the phase fluctuations, leading to a positive correction to the conductance. A non-perturbative theory of these fluctuations is required to quantitatively explain the very strong contribution of superconducting fluctuations to conductivity near the critical $V_g = -3$ V.

Superconducting glassy state

Another route to induce a quantum phase transition to the normal state in our superconducting array consists in applying a perpendicular magnetic field, H. The destruction of the array superconductivity by the magnetic field—we consider here a magnetic field smaller than the critical field of tin discs—results from the interplay between three different effects. First, the magnetic field imposes phase frustration between the discs. This frustration, which is given by $f = HS_0/\Phi_0$ ($S_0 = \sqrt{3}b^2/2$ is the area of the array elementary cell in the triangular lattice and $\Phi_0 = h/2e$ the flux quantum), impedes reaching a set of phase differences between discs, which simultaneously minimizes the Josephson energy of all junctions. Second, the magnitude of each individual Josephson coupling E_J^{ij} between two neighbouring discs i and j decreases with increasing magnetic field in a way such that the average $\langle E_J^{ij} \rangle$ drops exponentially beyond the magnetic length $L_H = \sqrt{\Phi_0/H}$, owing to random magnetic field-induced phase shifts, whereas the typical modulus of E_J^{ij} is suppressed by a factor of only $\sim 1/g$ (ref. 39).

Thereby both these effects converge to suppress superconductivity in the array. The second effect, however, leads to the enhancement of quantum phase fluctuations by mitigation of the proximity effect[17], whereas frustration may yield non-monotonic behaviour of the resistance with increasing H, as observed in tunnelling Josephson junction arrays[13,14].

The third effect to consider here comes from the phase coherent nature of the disordered graphene electron gas. As a result of the multiple interference of electron wavefunctions, the graphene conductance undergoes mesoscopic fluctuations that lead, in the normal state, to universal conductance fluctuations. In our proximity-coupled array, such mesoscopic fluctuations are present together with superconducting fluctuations, resulting in resistance fluctuations on varying electron density, as apparent in the gate evolution of the resistance measured at 0.06 K shown in Fig. 2a. In a similar fashion, small variations of the magnetic field can randomly modulate the Andreev conductance of each Josephson junction

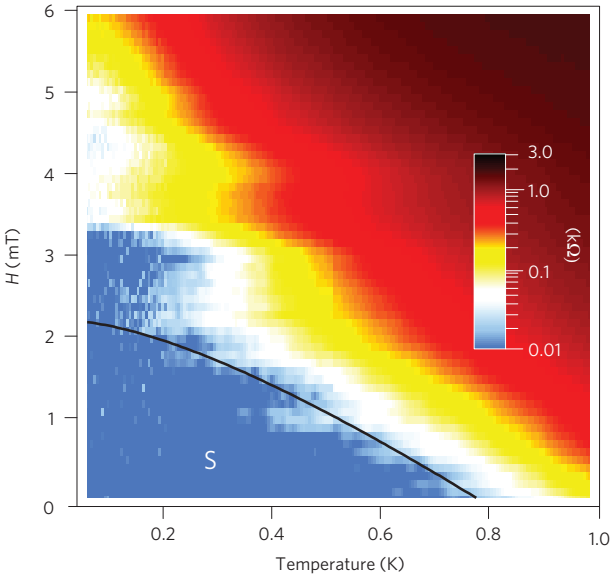

Figure 4 | Re-entrant superconductivity under a magnetic field. Colour-scaled map of the magnetoresistance (H) plotted as a function of temperature and magnetic field measured in the superconducting phase ($V_g = 30$ V). The upper critical field of the array is indicated by the white contour bordering the superconducting and resistive state. The solid line is a fit of the upper critical field by the BCS theory for dirty superconductors. A clear deviation occurs below 0.2 K, where a re-entrant pocket of superconductivity persists up to 3.3 mT and is followed at higher field by not-fully superconducting pockets, non-periodic in the magnetic field.

by dephasing the electron interference pattern[27,39,40], and therefore play an important role in the setting of global phase coherence, especially when the mean critical current is strongly suppressed by the magnetic field.

The conjunction of these three effects has led to theoretical predictions that, at very low temperature, superconductivity may persist above the upper critical field, H_{c2}, in the form of an upturn[28,29] of the T-dependence of H_{c2}, or a possible re-entrant superconducting phase[27]. The resulting state is expected to be a superconducting phase glass owing to the phase frustration between discs and to mesoscopic fluctuations that arbitrarily affect each Josephson coupling.

To address these fundamental aspects, we systematically measured the temperature evolution of the magneto-resistance of the sample in the superconducting phase far from the charge neutrality point ($V_g = 30$ V). Figure 4 presents the whole set of data in the form of a plot showing the colour-coded magneto-resistance as a function of T and H. The dark blue area indicates vanishingly small resistance—that is, the superconducting state—and the other colours indicate the resistive normal state. Interestingly, we observe that the superconducting phase extends over a wide and continuous range of magnetic field, which resembles the mixed phase of bulk superconductors. The temperature evolution of H_{c2} from 0.8 K down to 0.2 K indeed follows closely the theoretical behaviour of type-II superconductor[26], which we have traced as a black line in Fig. 4. At this gate voltage, the zero-temperature extrapolation of this theoretical fit gives 2.2 mT, which is close to full frustration $f = 1$ reached at the field value $H_{c0} = \Phi_0/S_0 = 2.3$ mT, that is, one flux quantum per unit cell.

However, inspecting Fig. 4 for T below 0.2 K, we observe that the experimental $H_{c2}(T)$ curve deviates upwards and shows a resilient superconducting pocket persisting up to 3.3 mT. Aperiodic replicas of different sizes, although of finite resistivity, are even visible at higher magnetic field. Importantly, in this re-entrant superconducting phase, the supercurrent is strongly suppressed

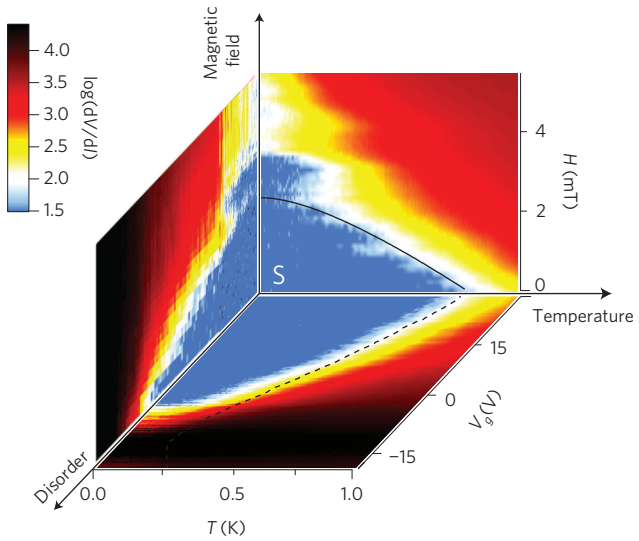

Figure 5 | Phase diagram of the superconductor-to-metal transition. A 3D-phase diagram showing the superconducting state reconstructed from three colour-scaled maps of the array resistance in (V_g,H,T) space. The resistance in (V_g,H) space is measured at 0.06 K. As the gate voltage V_g has a direct action on the effective disorder of the graphene mediating superconductivity, this axis has been relabelled accordingly. Notice the re-entrance of superconductivity above the first critical field, which can be seen in both the (V_g,H) and (H,T) planes.

in comparison with the main superconducting region at the same temperature (Supplementary Fig. 5). These observations agree with the theoretically expected dependence and support the existence of a superconducting phase glass state[27–29]. Such an experimental demonstration of re-entrant superconductivity in an inhomogeneous 2D superconducting system provides another fundamental aspect of proximity-coupled Josephson arrays.

Phase diagram of the quantum superconductor-to-metal transitions

The use of graphene here has provided a unique opportunity to explore in a single device the phase diagram in phase-space variables T, H and V_g, where V_g is equivalent to disorder, which drive the thermal and the quantum phase transitions to the normal state. Owing to the continuous tuning of disorder through the gate-tunable graphene electron density, we can therefore construct the entire phase diagram of the proximity-coupled Josephson junction array. The result shown in Fig. 5 provides a complete picture of the experimental temperature, disorder and magnetic field-driven superconductor-to-metal transitions addressed in this work.

The similarities to the original phase diagram based on the dirty-boson model[41] are striking and show that our proximity-coupled array behaves in many respects as disordered superconducting thin films. However, the new physical ingredient here relies on the inhomogeneous nature of superconductivity, which presents built-in superconducting discs subject to phase fluctuations. Such inhomogeneities also emerge close to the quantum critical point in amorphous thin films[42] in the form of self-induced fluctuations of the superconducting state induced by disorder[43].

To conclude, our work demonstrates that, by increasing the normal metal resistance in a proximity-coupled array, strong enhancement of quantum phase fluctuations terminates the superconducting state, leading to a metallic state, which markedly suppresses the critical temperature T_c. The use of graphene as a 2D electron gas platform has enabled us to continuously map the entire disorder and magnetic field-driven superconductor-to-metal transition. This plot evinces the appearance of a re-entrant superconductivity in the presence of a magnetic field above the critical field, in agreement with the predicted phase glass state. This system reveals the pronounced impact of quantum fluctuations induced by weak charge quantization in 2D superconducting systems.

Methods

We used CVD-grown monolayer graphene sheets transferred onto 285 nm oxidized silicon wafer as a 2D diffusive metal. As shown in Fig. 1, the sample was patterned by standard e-beam lithography into a Hall bar geometry (central square area 6 μm^2) and contacted with normal leads (Ti/Au bilayers, 5 nm/50 nm thick). The entire graphene surface was then decorated in a second lithography step by an array of 50-nm-thick Sn discs.

Samples were anchored to the mixing chamber of a ^{3}He–^{4}He dilution refrigerator placed inside a shielded cryostat and connected to highly filtered lines. Lossy coaxial lines, capacitive filters and π-filters were installed between the measurement apparatus and the mixing chamber stage of the refrigerator to strongly attenuate electronic noise above 10 kHz. A low-frequency lock-in measurement set-up based on the current bias method (2–5 nA input current) was used to measure the differential resistance while the voltage across the sample was measured with low-noise preamplifiers.

To fit T_{BKT} in the measured data in Fig. 2b, we substituted in equation (1) the Josephson couplings E_J found on the left side of equation (5) in ref. 29, which is the Josephson energy derived from the collective Josephson coupling in a 2D array using the Matsubara-space Usadel equation, with the result:

$$E_J(b,T) = 4\pi g T \sum_{\omega_n>0} \left\{ \pi / [2\ln(\sqrt{D/2\omega_n}/a)] \right\}^2 P(\sqrt{\omega_n/2E_{Th}}) \quad (3)$$

The above equation (3), together with equation (1), can be reduced to:

$$6\pi g \sum_{0}^{\infty} \frac{\pi^2}{\ln^2(\hbar D/2a^2\omega_n)} P(\sqrt{\omega_n/2E_{Th}}) = 1 \quad (4)$$

where $E_{Th} = (\hbar D/b^2)$ is the Thouless energy of a pair of discs separated by distance b, a is the diameter of the superconducting discs and $\omega_n = \pi T(2n+1)$ is the nth Matsubara frequency at temperature T. The function $P(z) = z\int_0^\infty K_0(z\cosh t)K_1(z\cosh t)\mathrm{d}t$, with $K_n(x)$ the MacDonald–Bessel function. Equation (4) contains only one variable, which is the critical temperature T at the BKT transition, as the parameters of g and D can be obtained from measured data. By summing equation (4) (high orders of n do not affect the sum significantly because the function P decays rapidly with increasing n), one gets the dashed line as the unique solution of equation (4) from the experimentally extracted g and D.

Received 05 October 2013; accepted 25 February 2014; published online 30 March 2014

References

1. Goldman, A. M. & Marković, N. Superconductor–insulator transitions in the two-dimensional limit. *Phys. Today* **51,** 39–44 (November 1998).
2. Dobrosavljevic, V., Trivedi, N. & Valles Jr, J. M. *Conductor–Insulator Quantum Phase Transitions* (Oxford Univ. Press, 2012).
3. Jaeger, H. M., Haviland, D. B., Orr, B. G. & Goldman, A. M. Onset of superconductivity in ultrathin granular metal films. *Phys. Rev. B* **40,** 182–196 (1989).
4. Allain, A., Han, Z. & Bouchiat, V. Electrical control of the superconducting-to-insulating transition in graphene-metal hybrids. *Nature Mater.* **11,** 590–594 (2012).
5. Ephron, D., Yazdani, A., Kapitulnik, A. & Beasley, M. R. Observation of quantum dissipation in the vortex state of a highly disordered superconducting thin film. *Phys. Rev. Lett.* **76,** 1529–1532 (1996).
6. Mason, N. & Kapitulnik, A. Dissipation effects on the superconductor–insulator transition in 2D superconductors. *Phys. Rev. Lett.* **82,** 5341–5344 (1999).
7. Mason, N. & Kapitulnik, A. Superconductor–insulator transition in a capacitively coupled dissipative environment. *Phys. Rev. B* **65,** 220505(R) (2002).
8. Qin, Y., Vicente, C. L. & Yoon, J. Magnetically induced metallic phase in superconducting tantalum films. *Phys. Rev. B* **73,** 100505(R) (2006).
9. Aubin, H. *et al.* Magnetic-field-induced quantum superconductor–insulator transition in $Nb_{0.15}Si_{0.85}$. *Phys. Rev. B* **73,** 094521 (2006).
10. Lin, Y-H., Nelson, J. & Goldman, A. M. Suppression of the Berezinskii–Kosterlitz–Thouless transition in 2D superconductors by macroscopic quantum tunneling. *Phys. Rev. Lett.* **109,** 017002 (2012).

11. Caviglia, A. D. *et al.* Electric field control of the $LaAlO_3/SrTiO_3$ interface ground state. *Nature* **456,** 624–627 (2008).
12. Biscaras, J. *et al.* Multiple quantum criticality in a two-dimensional superconductor. *Nature Mater.* **12,** 542–548 (2013).
13. Van der Zant, H. S. J., Fritschy, F. C., Elion, W. J., Geerligs, L. J. & Mooij, J. E. Field-induced superconductor-to-insulator transitions in Josephson-junction arrays. *Phys. Rev. Lett.* **69,** 2971–2974 (1992).
14. Van der Zant, H. S. J., Elion, W. J., Geerligs, L. J. & Mooij, J. E. Quantum phase transitions in two dimensions: Experiments in Josephson-junction arrays. *Phys. Rev. B* **54,** 10081–10093 (1996).
15. Abrahams, E., Anderson, P. W., Licciardello, D. C. & Ramakrishnan, T. V. Scaling theory of localization: absence of quantum diffusion in two dimensions. *Phys. Rev. Lett.* **42,** 673–676 (1979).
16. Feigel'man, M. V. & Larkin, A. I. Quantum superconductor-metal transition in a 2D proximity coupled array. *Chem. Phys.* **235,** 107–114 (1998).
17. Feigel'man, M. V., Larkin, A. I. & Skvortsov, M. A. Quantum superconductor–metal transition in a proximity array. *Phys. Rev. Lett.* **86,** 1869–1872 (2001).
18. Das, D. & Doniach, S. Existence of a Bose metal at T = 0. *Phys. Rev. B* **60,** 1261–1275 (1999).
19. Kapitulnik, A., Mason, N., Kivelson, S.A. & Chakravarty, S. Effects of dissipation on quantum phase transitions. *Phys. Rev. B* **63,** 125322 (2001).
20. Spivak, B., Zyuzin, A. & Hruska, M. Quantum superconductor–metal transition. *Phys. Rev. B* **64,** 132502 (2001).
21. Phillips, P. & Dalidovitch, D. The elusive Bose metal. *Science* **302,** 243–247 (2003).
22. Spivak, B., Oreto, P. & Kivelson, S. A. Theory of quantum metal to superconductor transitions in highly conducting systems. *Phys. Rev. B* **77,** 214523 (2008).
23. Feigelman, M. V., Kamenev, A., Larkin, A. I. & Skvortsov, M. A. Weak charge quantization on a superconducting island. *Phys. Rev. B* **66,** 054502 (2002).
24. Eley, S., Gopalakrishnan, S., Goldbart, P. M. & Mason, N. Approaching zero-temperature metallic states in mesoscopic superconductor–normal–superconductor arrays. *Nature Phys.* **8,** 59–62 (2012).
25. Geim, A. K. & Novoselov, K. S. The rise of graphene. *Nature Mater.* **6,** 183–191 (2007).
26. De Gennes, P. G. *Superconductivity of Metals and Alloys* (Addison-Wesley, 1989).
27. Spivak, B. & Zhou, F. Mesoscopic effects in disordered superconductors near H_{c2}. *Phys. Rev. Lett.* **74,** 2800–2003 (1995).
28. Galitski, V. M. & Larkin, A. I. Disorder and quantum fluctuations in superconducting films in strong magnetic fields. *Phys. Rev. Lett.* **87,** 087001 (2001).
29. Feigel'man, M. V., Skvortsov, M. A. & Tikhonov, K. S. Proximity-induced superconductivity in graphene. *Pis'ma v ZhETF* **88,** 780–784 (2008); *JETP Lett.* **88,** 747–751 (2008).
30. Kessler, B. M., Girit, C. Ö, Zettl, A. & Bouchiat, V. Tunable superconducting phase transition in metal-decorated graphene sheets. *Phys. Rev. Lett.* **104,** 047001 (2010).
31. Resnick, D. J., Garland, J. C., Boyd, J. T., Shoemaker, S. & Newrock, R. S. Kosterlitz–Thouless transition in proximity-coupled superconducting arrays. *Phys. Rev. Lett.* **47,** 1542–1545 (1981).
32. Abraham, D. W., Lobb, C. J., Tinkham, M. & Klapwijk, T. M. Resistive transition in two-dimensional arrays of superconducting weak links. *Phys. Rev. B* **26,** 5268–5271 (1982).
33. Huard, B., Stander, N., Sulpizio, J. A. & Goldhaber-Gordon, D. Evidence of the role of contacts on the observed electron–hole asymmetry in grapheme. *Phys. Rev. B* **78,** 121402(R) (2008).
34. Berezinskii, V. L. Violation of long range order in one-dimensional and two-dimensional systems with a continuous symmetry group: I Classical systems. *Zh. Eksp. Teor. Fiz.* **59,** 907–920 (1970); *Sov. Phys. JETP* **32,** 493–500 (1971).
35. Kosterlitz, J. M. & Thouless, D. Ordering, metastability and phase transitions in two-dimensional systems. *J. Phys. C* **6,** 1181–1203 (1973).
36. Aslamazov, L. G. & Larkin, A. I. Effect of fluctuations on the properties of a superconductor above the critical temperature. *Fiz. Tv. Tela* **10,** 1104–1111 (1968); *Sov. Phys. Solid State* **10,** 875–880 (1968).
37. Maki, K. Critical fluctuation of the order parameter in a superconductor. *Progr. Theor. Phys.* **40,** 193–200 (1968).
38. Thompson, R. S. Microwave, flux flow, and fluctuation resistance of dirty Type-II superconductors. *Phys. Rev. B* **1,** 327–333 (1970).
39. Al'tshuler, B. L. & Spivak, B. Z. Mesoscopic fluctuations in a superconductor-normal metal-superconductor junction. *Zh. Eksp. Teor. Fiz.* **92,** 609–615 (1987); *Sov. Phys. JETP* **65,** 343–347 (1987).
40. Den Hartog, S. G. *et al.* Sample-specific conductance fluctuations modulated by the superconducting phase. *Phys. Rev. Lett.* **76,** 4592–4595 (1996).
41. Fisher, M. P. A. Quantum phase transitions in disordered two-dimensional superconductors. *Phys. Rev. Lett.* **65,** 923–926 (1990).
42. Finkel'shtein, A.M. Superconducting transition temperature in amorphous films. *Pisma ZhETF* **45,** 37–40 (1987); *JETP Lett.* **45,** 46–49 (1987).
43. Skvortsov, M. A. & Feigel'man, M. V. Superconductivity in disordered thin films: giant mesoscopic fluctuations. *Phys. Rev. Lett.* **95,** 057002 (2005).

Acknowledgements

Samples were fabricated at the NANOFAB facility of the Néel Institute, the technical team of which has been of critical help for this work. We thank D. Shahar for valuable discussions and comments on the manuscript. We thank N. Bendiab, H. Bouchiat, C. Chapelier, J. Coraux, C. O. Girit, B. M. Kessler, L. Marty, A. Reserbat-Plantey and A. Zettl for stimulating discussions. This work is financially supported by ANR-BLANC projects SuperGraph, TRICO and Cleangraph, and DEFI Nano ERC Advanced Grant MolNanoSpin. Z.H. and H.A-T. acknowledge PhD grant support from the Cible program of Région Rhone-Alpes and from Nanosciences Foundation Grenoble respectively. The research of M.F. is partially supported by RFBR grant no 13-02-00963.

Author contributions

Z.H., A.A., M.F., B.S. and V.B. conceived and designed the experiments. Z.H., H.A-T. and V.B. performed the experiments. Z.H., B.S., K.T., A.A. and M.F. contributed to the materials/analysis tools. Z.H., B.S., M.F., K.T. and V.B. analysed the data and wrote the paper.

Additional information

Supplementary information is available in the online version of the paper. Reprints and permissions information is available online at www.nature.com/reprints. Correspondence and requests for materials should be addressed to V.B.

Competing financial interests

The authors declare no competing financial interests.